ORIGINAL RESEARCH

Exploring the Nicotinic Acetylcholine Receptor-associated Proteome with iTRAQ and Transgenic Mice

Tristan D. McClure-Begley [1,2], Kathy L. Stone [3], Michael J. Marks [2,4],
Sharon R. Grady [2], Christopher M. Colangelo [3,5], Jon M. Lindstrom [6],
Marina R. Picciotto [1,*]

[1] *Department of Psychiatry, Yale University School of Medicine, New Haven, CT 06508, USA*
[2] *Institute for Behavioral Genetics, University of Colorado, Boulder, CO 80303, USA*
[3] *W.M. Keck Biotechnology Resource Laboratory, Yale University School Medicine, New Haven, CT 06509, USA*
[4] *Department of Psychology and Neuroscience, University of Colorado, Boulder, CO 80309, USA*
[5] *Department of Molecular Biophysics & Biochemistry, Yale University, New Haven, CT 06520, USA*
[6] *Department of Neuroscience, Medical School of the University of Pennsylvania, Philadelphia, PA 19104, USA*

Abstract Neuronal nicotinic acetylcholine receptors (nAChRs) containing α4 and β2 subunits are the principal receptors in the mammalian central nervous system that bind nicotine with high affinity. These nAChRs are involved in nicotine dependence, mood disorders, neurodegeneration and neuroprotection. However, our understanding of the interactions between α4β2-containing (α4β2*) nAChRs and other proteins remains limited. In this study, we identified proteins that interact with α4β2* nAChRs in a gene-dose dependent pattern by immunopurifying β2* nAChRs from mice that differ in α4 and β2 subunit expression and performing proteomic analysis using isobaric tags for relative and absolute quantitation (iTRAQ). Reduced expression of either the α4 or the β2 subunit results in a correlated decline in the expression of a number of putative interacting proteins. We identified 208 proteins co-immunoprecipitated with these nAChRs. Furthermore, stratified linear regression analysis indicated that levels of 17 proteins was correlated significantly with expression of α4β2 nAChRs, including proteins involved in cytoskeletal rearrangement and calcium

* Corresponding author.
  E-mail: marina.picciotto@yale.edu (Picciotto MR).

Production and hosting by Elsevier

signaling. These findings represent the first application of quantitative proteomics to produce a β2* nAChR interactome and describe a novel technique used to discover potential targets for pharmacological manipulation of α4β2 nAChRs and their downstream signaling mechanisms.

Introduction

Neuronal nicotinic acetylcholine receptors (nAChRs) are involved in a wide variety of functions in the central nervous system (CNS) and are disrupted in several psychiatric and neurological disorders. The most abundant high-affinity nAChRs in the mammalian CNS contain the α4 and β2 subunits [1–3] and this receptor subtype represents an important target for studies of functionally relevant protein–protein interactions. Heteromeric α4β2* nAChRs (where * denotes other, potentially unidentified, subunits) bind nicotine with high affinity [4,5] and are targeted by pharmacotherapies for smoking cessation [6], Alzheimer's disease [7], Parkinson's disease [8], mood disorders [9] and attention deficit hyperactivity disorder (ADHD) [10]. A better understanding of the nAChR signaling complex could lead to a better drug design to achieve desired therapeutic effects.

A number of studies have elucidated regulatory mechanisms that modulate nAChR function and cellular trafficking. The interaction of 14-3-3 adaptor proteins with α4 subunit affects the stoichiometry and agonist sensitivity of α4β2 nAChRs [11,12]. Interactions with the calcium-sensor protein VILIP-1 affect the agonist sensitivity and assembly of α4* nAChRs [13]. Phosphorylation of α4 subunit by protein kinase A (PKA) affects association with 14-3-3 adaptor proteins and regulate α4β2 nAChR assembly [12,14]. Phosphorylation by protein kinase C (PKC) and dephosphorylation by the phosphatase calcineurin alter the transition of α4β2 nAChRs into and out of functionally desensitized states following prolonged exposure to agonists [15–17]. Although these studies, and others, have identified protein–protein interactions with α4β2 nAChRs, our knowledge of the receptor interactome remains incomplete.

Mass spectrometry (MS)-based proteomic analysis allows simultaneous identification of multiple proteins present in varying quantities in complex mixtures. The ability of MS to obtain accurate peptide sequences, and subsequently identify proteins from these detected unique sequences using protein databases, has been a significant technological advance providing high-throughput accurate protein profiling (see [18,19] for review). A set of proteins that appear to be associated with β2* nAChRs were identified previously by analyzing proteins isolated from the mouse brain tissue using a β2-selective monoclonal antibody (mAb270) and MS with matrix-assisted laser desorption and tandem time-of-flight (MALDI–ToF-ToF) followed by comparison to complexes in β2 subunit null-mutant mice [20]. This study demonstrated the utility of MS to detect nAChR-interacting proteins from the brain tissue. However, no quantitative methods have been employed to address specificity of the interaction between the identified proteins and the β2* nAChRs, as well as their partner subunits.

Stable isotopic labeling in cell culture (SILAC) has been used to identify highly specific protein–protein interactions. Selective protein was knocked down via siRNA in cultured cells grown in standard media, in comparison with cells grown in media supplemented with "heavy" amino acids [21,22]. However, this technique is limited by its capacity to compare only two samples, and stable isotopic labeling is not currently feasible for tissue homogenates. In contrast, label-free based quantitative MS is performed sequentially and thus introduces run-to-run variations in peptide elution, preventing accurate quantitation between sample sets. In order to facilitate identification of nAChR-interacting proteins with high confidence, we performed quantitative proteomic analysis using isobaric tags for relative and absolute quantitation (iTRAQ) [23]. iTRAQ reduces variation by labeling multiple protein samples and mixing these samples together prior to liquid chromatography–tandem MS (LC–MS/MS) analysis, enabling identification and quantitation of multiple proteins from several samples concurrently [24].

In this study, we combined the iTRAQ technique with the use of α4 and β2 nAChR subunit null-mutant mouse lines (these null-mutants express no functional α4β2 nAChRs [4,25] and heterozygotes express intermediate levels [26]). A β2 subunit specific monoclonal antibody was used to isolate the receptors and quantify gene dose-dependent changes in the α4β2* nAChR interactome. The ability of iTRAQ to multiplex all six genotypes in a single LC–MS/MS experiment is essential for the quantitative identification and comparison of interacting proteins across genotypes. This integrated strategy recapitulates powerful cell-based techniques, but capitalizes on the ability of iTRAQ to label multiple *ex vivo* tissue samples. This technique identified a group of proteins that are associated linearly with mature nAChRs expressed in the mammalian brain and provided a platform for exploring functional relevance of this interactome.

Results

Characterizing quantitative mAb295-M270 solid phase immunodepletion of β2* nAChRs from mouse brain

We first generated mAb295-coupled M270 Dynabeads using 0.5, 1, 2 or 5 µg of mAb295/mg of M270 beads in order to determine the optimal concentration of beads as well as the optimal ratio of bead suspension to brain extracts for quantitative immunoprecipitation of β2* nAChRs. Increasing volumes (0, 1.56, 3.125, 6.25, 12.5, 25, 50, 100 µl) of bead suspension from each concentration of mAb295 were used to capture β2* nAChRs labeled with 1 nM [³H]-epibatidine. Brain samples of three C57BL/6 mice were solubilized. After centrifugation, supernatants were pooled, and 100 µl aliquots were used in triplicate for each concentration of mAb295 across all eight bead volumes to measure the efficiency and extent of [³H]-epibatidine binding site capture. Depletion of [³H]-epibatidine binding from mouse brain extracts by immobilized mAb295 was saturable and nearly complete across all four concentrations of mAb295 tested (Figure S1A). The ½ maximal bead volume for nAChR capture decreased with increasing concentrations of mAb295 ($R^2 = 0.83$; Figure S1B), but the calculated maximal binding site capture was not significantly different across the four mAb295-M270 bead ratios

$(F_{(3, 11)} = 1.23, P = 0.36)$. This suggests that the amount of mAb295 coupled to the magnetic beads is more important for efficient capture of β2* nAChRs than the total available surface area of the beads themselves. Therefore, under the conditions outlined in this experiment, steric hindrance of protein complexes adhering to the nAChRs was not likely to affect the ability of the mAb295-M270 beads to trap solubilized β2* nAChRs and their associated protein complexes from brain extracts effectively. Calculated parameters for specific capture of [³H]-epibatidine binding sites by mAb295-M270 beads are presented in Table S1.

Immunopurification of β2* nAChRs from brain tissue of α4 or β2 subunit transgenic mice

Using optimal conditions (5 µg mAb295/mg M270 beads; bead volume 10% of total extracts), we extracted β2* nAChRs from mouse brain extracts prepared from wild type (WT), heterozygous (HET) and homozygous (KO) mice lacking either α4 or β2 nAChR subunit. There was a gene dose-dependent effect on the number of total [³H]-epibatidine binding sites in brain detergent extracts (Table 1) across genotypes. There was no significant binding site capture from brains of α4 KO or β2 KO mice. No significant difference was detected in the percentage of binding sites captured from tissue samples of WT and HET α4 (79.6 ± 5.4 vs 83.1 ± 7.5%; $n = 3$, $P = 0.72$, t-test) or β2 (79.3 ± 0.9 vs 78.8 ± 1.3%; $n = 3$, $P = 0.78$, t-test), indicating that immobilized mAb295 performed similarly in all samples regardless of nAChR protein content.

Measurement of relative expression of nAChR subunit proteins by iTRAQ and LC–MS/MS

Quantitation of iTRAQ measured abundance is expressed as the $\log_2$ of the ratio of mean reporter ion peak areas ($\log_2$MRIPA) of all proteins present in all samples relative to the average WT abundance of the β2 nAChR subunit (the target of the IP). Since α4 and β2 nAChR subunit levels vary with gene dose, we evaluated their levels in each sample to judge the ability of iTRAQ to quantify proteins in immunocaptured eluates. Although [³H]-epibatidine binding sites varied with α4 and β2 genotypes, total protein eluted following immunoprecipitation (IP) did not differ significantly across genotypes ($F_{(5, 17)} = 2.52$, $P = 0.09$). However, $\log_2$MRIPA ratio of β2 nAChR subunit was significantly affected by nAChR subunit knockout in a gene dose-dependent fashion (mean $\log_2$MRIPA ± SEM; α4 WT: 0.12 ± 0.17, HET: −0.31 ± 0.16, KO: −0.94 ± 0.23; $F_{(2, 8)} = 7.39$, $P = 0.024$; one-way ANOVA. β2 WT: −0.19 ± 0.23, HET: −0.60 ± 0.31, KO: −1.53 ± 0.19; $F_{(2, 8)} = 8.35$, $P = 0.018$; one-way ANOVA). However, although the $\log_2$MRIPA ratio for α4 subunit was

significantly affected by α4 subunit knockout in a gene dose-dependent fashion (mean $\log_2$MRIPA ± SEM; WT: 0.09 ± 0.25, HET: −0.46 ± 0.39, KO: −1.44 ± 0.05; $F_{(2, 8)} = 9.34$, $P = 0.014$; one-way ANOVA), such alteration was not obviously observed in β2 subunit knockout mice (WT: −0.21 ± 0.33, HET: −0.42 ± 0.23, KO: −1.40 ± 0.43; $F_{(2, 8)} = 3.27$, $P = 0.1$; one-way ANOVA; Figure 1). $\log_2$MRIPA was correlated positively with [³H]-epibatidine binding sites captured by immobilized mAb295 for both α4 ($R^2 = 0.80$, $P < 0.0009$) and β2 subunit ($R^2 = 0.65$, $P < 0.0009$), indicating that $\log_2$MRIPA ratio for each subunit is a reliable measure of the assembled nAChRs in each sample. The data for α4 and β2 WT, HET and KO mice appear as three distinct groupings along the regression line (Figure 2).

It should be noted that the $\log_2$MRIPA ratio measures the relative abundance of labeled peptides using a control sample as a reference. In fact, peptides that uniquely identify β2 and α4 nAChR subunits were detected in the subunit KO brain tissue, despite the lack of [³H]-epibatidine binding. These data are consistent with the fact that neither β2 nor α4 knockout completely abolishes the entire extracellular domain of the β2 nAChR subunit that is specifically recognized by mAb295 [4,25]. Thus, although these nAChR subunit knockouts completely eliminate nicotinic agonist binding sites and functional nAChRs, a small amount of a non-functional protein appears to be produced that is able to form some complexes with interacting proteins.

Defining and stratifying an α4β2* nAChR interactome by multiple linear regression following iTRAQ LC–MS/MS

We performed multiple linear regression on the positively identified proteins in the three biological replicates to identify highly specific interacting peptides whose relative abundance changes proportionally with the amount of quantitated nAChRs. Included proteins were identified by more than one significant and unique peptide (peptide expectation score < 1.7, corresponding to a confidence interval of 95%) in at least one biological replicate. There were 208 proteins identified by LC–MS/MS acquired, iTRAQ labeled peptides, with linear correlation coefficients ranging from +1 for β2 nAChR subunit to −0.847 for vesicle-associated membrane protein 2 (VAMP2) (Table S2).

Identification of significant α4β2* interacting proteins

We did not fractionate tissue prior to processing, which maximized β2* nAChR content, but also introduced proteins from irrelevant cellular compartments that formed complexes with the immunopurified nAChRs. Some proteins appeared to be

Table 1 Gene dose-dependent effect on the number of [³H]-epibatidine binding sites of nAChRs

Number of [³H]-epibatidine binding sites (fmol)		Genotype			$F_{(2, 8)}$ score	P value
	nAChR subunit	WT	HET	KO		
Total in brain extracts (mean ± SEM)	α4	609.3 ± 101.5	514.0 ± 109.0	51.9 ± 4.5	12.00	0.008
	β2	633.6 ± 124.0	463.6 ± 2.6	38.9 ± 9.7	18.17	0.003
Captured by immobilized mAb295 (mean ± SEM)	α4	522.7 ± 120.3	420.3 ± 116.8	−1.0 ± 12.2	8.18	0.019
	β2	505.6 ± 103.5	365.2 ± 6.5	−5.0 ± 10.5	19.21	0.002
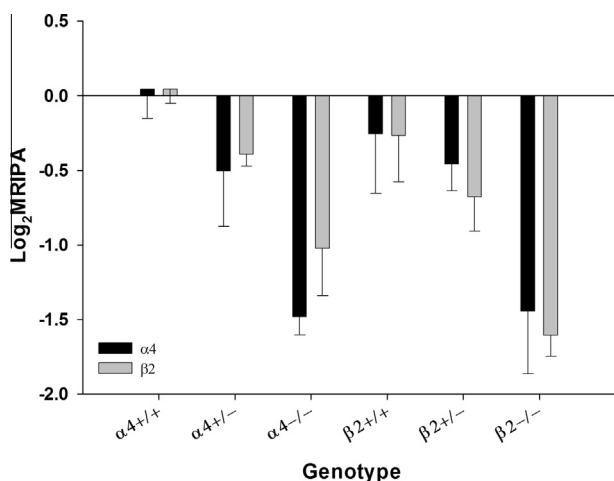
Figure 1 Gene dose-dependent effects of nAChR subunit gene deletion on the relative protein abundance of α4 and β2 subunits
The relative abundance of α4 and β2 nAChR subunits determined by iTRAQ quantitation of the $\log_2$ mean reporter ion peak areas ($\log_2$MRIPA) is significantly altered as measured by an overall ANOVA by the full or partial gene deletion of either subunit (α4: $n = 9$, $F_{(2, 8)} = 7.39$, $P = 0.024$; β2: $n = 9$, $F_{(2, 8)} = 8.35$, $P = 0.018$). Gene dose-dependent decreases in abundance demonstrate the interdependence of α4 and β2 nAChR subunits in mouse brain. MRIPA stands for mean reporter ion peak area.
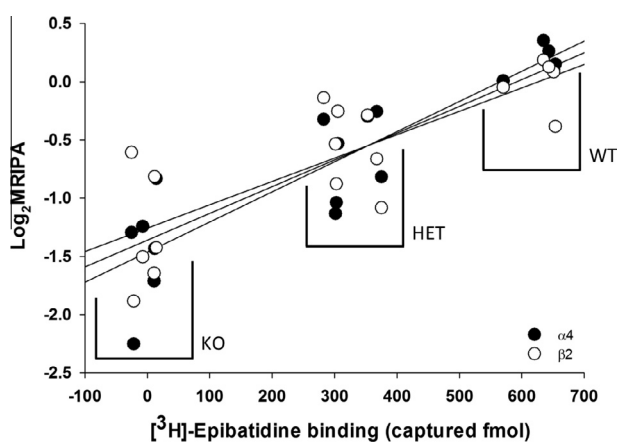
Figure 2 Correlation of nAChR abundance measured by iTRAQ and ligand binding
Correlation between fmol of [³H]-epibatidine binding and measured $\log_2$MRIPA of α4 and β2 was plotted. The relative abundance of α4 (black circles) and β2 (white circles) nAChR subunits measured by iTRAQ follow a gene-dose dependent decrease and is significantly correlated with [³H]-epibatidine binding across the six genotypes examined (WT, HET and KO; α4: $r = 0.894$, $P < 0.0009$; β2: $r = 0.804$, $P < 0.0009$).

associated quite strongly ($r > 0.5$ using Pearson's product moment correlation coefficient since the relationship between nAChR subunit gene dose and receptor expression is linear) with β2* nAChRs (such as certain histone isoforms), despite the fact that nAChRs would not be expected to localize to

the nucleus or mitochondria. The UniProt Knowledgebase (UniProtKB) [27] was therefore used to cull proteins from the list when the assigned cellular compartment did not correspond to sites of known nAChR localization. Exceptions were made in the case of two transcription factors: Pur-α, which has the capacity to translocate from the cytosol to the nucleus [28], and thyroid hormone receptor-associated protein 3 (THRAP3), which we previously identified in an additional unpublished nAChR interactome study. Additional analysis focused only on 91 proteins in these compartments, with 62 identified as cytoplasmic, 26 associated with the plasma membrane and the remaining 3 proteins associated with the Golgi apparatus/endomembrane system (**Table 2**). Of these, only 17 proteins (11 cytoplasmic and 6 associated with the plasma membrane) showed statistically significant correlation with levels of the β2 nAChR subunit (**Table 3**). Classification of these 17 proteins with PANTHER Gene Ontology (GO) of molecular function [29] revealed distinct biological activity profiles (**Table 3**).

In the primary (unfiltered) dataset, distribution of correlation coefficients for β2 $\log_2$MRIPA was distinctly bimodal, with a major mode occurring between 0 and −0.5, and a minor mode occurring between 0.25 and 0.75 (**Figure 3**A). These data suggest that this dataset represents two sets of events: proteins that likely interacted with the antibody complex when it was not occupied by nAChRs ($r < 0$) and proteins that interacted selectively with the immunoprecipitated nAChRs ($r > 0.25$). In the secondary dataset, adjustment for cellular compartment eliminated the events with $r < 0$ and resulted in a unimodal distribution approximately equivalent to the minor mode with $r > 0.25$ (**Figure 3**B). These data suggest that eliminating the group of proteins that are not co-localized with the nAChRs in these cellular compartments also screens out the majority of proteins that interact non-specifically with the antibody complex. The tertiary dataset (selected for significant positive correlation with β2 nAChR subunit expression; $P < 0.05$) was also unimodal, with the majority of the distribution centered between 0.5 and 0.75 (**Figure 3**C). Eliminating proteins based on cellular compartments favored identification of more positive correlations with β2 nAChR subunit abundance. Such result is consistent with the observation that calculated kurtosis for the frequency distribution increased from an estimate of −0.513 to 1.211 when moving from the primary to secondary dataset, an indication that the selected datasets deviated significantly from chance. Indeed, all three frequency distributions were significantly different from a normal distribution according to Shapiro–Wilk test ($P = 0.006$, 0.021 and 0.022 for primary, secondary and tertiary dataset, respectively), indicating that the samples were substantially enriched for a particular target protein and the associated proteins identified were largely non-random.

Discussion

This study used quantitative protein identification with iTRAQ and LC–MS/MS to identify protein–protein interactions for α4β2 nAChRs. A highly specific monoclonal antibody was used to capture β2* nAChRs reliably and efficiently from detergent extracts of mouse brain homogenates, facilitating the identification of a set of putative nAChR-interacting proteins. Proteins of particular interest

Table 2   **Proteins specifically associated with nAChRs based on cellular compartments**

Correlation coefficient	N	F score	P value	Protein	UniProtKB accession No.	Cellular compartment	Previously identified?
0.185	18	0.568	0.462	14-3-3 protein ζ/δ	P63101	Cytoplasm	Yes
0.117	18	0.221	0.645	2′,3′-cyclic-nucleotide 3′-phosp hodiesterase	P16330	Cell membrane	Yes
0.326	18	1.909	0.186	Actin, alpha cardiac muscle 1	P68033	Cytoplasm	No
0.375	18	2.623	0.125	Actin, cytoplasmic 2	P63260	Cytoplasm	Yes
0.645	18	11.404	0.004	Actin-related protein 3	Q99JY9	Cytoplasm	No
0.37	18	2.536	0.131	α-actinin-1	Q7TPR4	Cytoplasm	No
0.104	12	0.11	0.747	α-actinin-2	Q9JI91	Cytoplasm	No
0.162	12	0.271	0.614	α-enolase	P17182	Cytoplasm	No
0.464	18	4.4	0.052	α-internexin	P46660	Cytoplasm	No
0.227	18	0.866	0.366	Ankyrin-2	Q8C8R3	Cytoplasm	No
0.021	12	0.005	0.948	Brain acid soluble protein 1	Q91XV3	Cell membrane	No
0.637	18	10.904	0.004	Calcium/calmodulin-dependent protein kinase type II subunit α	P11798	Cytoplasm	No
0.172	6	0.49	0.494	Calcium/calmodulin-dependent protein kinase type II subunit β	P28652	Cytoplasm	No
0.456	6	1.048	0.364	Calcium/calmodulin-dependent protein kinase type II subunit δ	Q6PHZ2	Cell membrane	No
0.917	18	21.235	0.01	Calcium/calmodulin-dependent protein kinase type II subunit γ	Q923T9	Sarcoplasmic reticulum membrane	No
0.235	18	0.938	0.347	Coronin-2B	Q8BH44	Cytoplasm	No
0.598	6	2.221	0.21	Dihydropyrimidinase-related protein 2	O08553	Cytoplasm	No
0.186	18	0.143	0.724	Disks large homolog 4	Q62108	Cell membrane	Yes
0.468	18	4.495	0.05	Drebrin	Q9QXS6	Cytoplasm	No
0.327	18	1.911	0.186	Dynein light chain 2, cytoplasmic	Q9D0M5	Cytoplasm	No
0.539	18	6.563	0.021	Ectonucleotide pyrophosphatase/ phosphodiesterase family member 6	Q8BGN3	Cell membrane	No
0.386	6	2.807	0.113	EF-hand domain-containing protein D2	Q9D8Y0	Membrane raft	No
0.57	18	7.681	0.014	F-actin-capping protein subunit α2	P47754	Cytoplasm	No
0.46	6	4.286	0.055	F-actin-capping protein subunit β	P47757	Cytoplasm	No
0.337	18	2.052	0.171	Gelsolin	P13020	Cytoplasm	No
0.748	12	20.268	0	Glial fibrillary acidic protein	P03995	Cytoplasm	No
0.476	18	2.937	0.117	Glutamine synthetase	P15105	Cytoplasm	No
0.417	18	3.371	0.085	Glyceraldehyde-3-phosphate dehydrogenase	P16858	Cytoplasm	Yes
0.045	18	0.033	0.859	Guanine nucleotide-binding protein G(o) subunit α	P18872	Heterotrimeric G-protein complex	Yes
0.193	18	0.622	0.442	Heat shock cognate 71 kDa protein	P63017	Cytoplasm	No
0.46	18	4.29	0.055	Heterogeneous nuclear ribonucleoprotein D0	Q60668	Nucleus	No
0.486	12	1.237	0.328	Heterogeneous nuclear ribonucleoprotein U	Q8VEK3	Nucleus	No
0.243	6	1.957	0.192	ʟ-Lactate dehydrogenase A chain	P16125	Cytoplasm	No
0.332	18	1.984	0.178	Myelin basic protein	P04370	Myelin membrane	Yes
0.332	18	1.984	0.178	Myelin basic protein	P04370	Myelin membrane	Yes
0.506	18	5.496	0.032	Myelin proteolipid protein	P60202	Cell membrane	No
0.262	18	1.183	0.293	Myosin light polypeptide 6	Q60605	Cytoplasm	No
0.512	18	5.695	0.03	Myosin-10	Q61879	Cytoplasm	No
0.085	18	0.117	0.737	Myosin-9	Q8VDD5	Cytoplasm	No
0.652	18	11.844	0.003	Neurofilament light polypeptide	P08551	Growth cone	No
0.379	18	2.683	0.121	Neurofilament medium polypeptide	P08553	Growth cone	No
0.858	18	44.542	0	Neuronal acetylcholine receptor subunit α4	O70174	Cell junction	No
1	18	–	0	Neuronal acetylcholine receptor subunit β2	Q9ERK7	Cell junction	No
0.02	18	0.006	0.938	Peptidyl-prolyl *cis–trans* isomerase A	P17742	Cytoplasm	No
0.431	6	2.279	0.162	Peroxiredoxin-1	P35700	Cytoplasm	No
0.484	12	3.061	0.111	Pyruvate kinase isozymes M1/M2	P52480	Cytoplasm	No
0.287	12	0.901	0.365	Ras-related protein Rab-11B	P46638	Cell membrane	No
0.397	6	1.867	0.202	Ras-related protein Rab-7a	P51150	Late endosome	No
0.31	12	1.063	0.327	Ras-related protein Ral-A	P63321	Cell membrane	No
0.856	6	11.009	0.029	Ras-related protein Rap-1A	P62835	Cell membrane	No
0.171	6	0.302	0.595	Ras-related protein Rap-1b	Q99JI6	Cell membrane	No
0.443	12	2.44	0.149	Serine/threonine-protein phosphatase PP1β catalytic subunit	P62141	Cytoplasm	No
0.69	6	3.633	0.129	Serine/threonine-protein phosphatase PP1γ catalytic subunit	P63087	Cytoplasm	No
0.224	12	0.529	0.484	Sodium/potassium-transporting ATPase subunit α2	Q6PIE5	Cell membrane	No

Table 2   continued

Correlation coefficient	N	F score	P value	Protein	UniProtKB accession No.	Cellular compartment	Previously identified?
0.261	18	1.169	0.296	Sodium/potassium-transporting ATPase subunit α3	Q6PIC6	Cell membrane	No
0.266	18	1.217	0.286	Sodium/potassium-transporting ATPase subunit β1	P14094	Cell membrane	No
0.502	18	5.378	0.034	Spectrin α chain, brain	P16546	Cytoplasm	Yes
0.519	18	5.884	0.027	Spectrin β chain, brain 1	Q62261	Cytoplasm	No
0.299	18	1.566	0.229	Synaptopodin	Q8CC35	Cytoplasm	No
0.547	12	4.265	0.066	Synaptotagmin-1	P46096	Cytoplasmic vesicle	No
0.536	12	4.026	0.073	Syntaxin-1B	P61264	Cell membrane	No
0.086	18	0.119	0.734	Syntaxin-binding protein 1	O08599	Cell membrane	No
0.562	18	7.386	0.015	Thyroid hormone receptor-associated protein 3	Q569Z6	Nucleus	No
0.665	12	7.933	0.018	Transcriptional activator protein Pur-α	P42669	Nucleus	No
0.491	6	1.272	0.322	Triosephosphate isomerase	P17751	Cytoplasm	No
0.334	18	2.011	0.175	Tropomodulin-2	Q9JKK7	Cytoplasm	No
0.451	18	4.087	0.06	Tubulin α-1A chain	P68369	Cytoplasm	Yes
0.431	18	3.652	0.074	Tubulin α-4A chain	P68368	Cytoplasm	No
0.422	18	3.466	0.081	Tubulin β-2A chain	Q7TM M 9	Cytoplasm	No
0.493	18	5.149	0.037	Tubulin β-3 chain	Q9ERD7	Cytoplasm	No
0.379	18	2.688	0.121	Tubulin β-4A chain	Q9D6F9	Cytoplasm	No
0.432	12	2.298	0.16	Tubulin β-5 chain	P99024	Cytoplasm	No
0.434	18	3.717	0.072	Unconventional myosin-Va	Q99104	Cytoplasm	No
0.295	18	1.52	0.235	Unconventional myosin-VI	Q64331	Golgi apparatus	No
0.01	12	0.001	0.975	Unconventional myosin-XVIIIa	Q9JMH9	ER-Golgi intermediate compartment	No
0.18	6	0.537	0.474	Vesicle-fusing ATPase	P46460	Cytoplasm	No
0.195	18	0.158	0.712	Vimentin	P20152	Cytoplasm	No
0.179	6	0.527	0.478	V-type proton ATPase catalytic subunit A	P50516	Cell membrane	No

Note: Correlation coefficient was calculated using Pearson's product moment; N indicates the number of samples contributing to analysis; F score was generated by one-way ANOVA.

were identified, amounts of which tend to follow a linear trend with respect to the measured quantity of α4β2* nAChRs that are present in the samples from WT, HET and KO mice transgenic for the α4 or β2 subunit. The $\log_2$MRIPA ratios (transformed representation of average protein abundance measured by iTRAQ) of the individual α4 and β2 nAChR subunit proteins were significantly correlated with the measured [³H]-epibatidine binding sites, supporting the accuracy and reproducibility of iTRAQ-coupled LC–MS/MS. Previous studies have shown that expression of α4 nAChR subunits is largely dependent on that of β2 subunit; however, low levels of β2* nAChRs remain in the absence of α4 [26,30]. Additional α subunits (α2, α3 and α6) are expressed in the CNS and can form functional nAChRs together with β2 subunits [31]. Although the non-α4 nAChRs are not sufficiently abundant to allow identification of these complexes from the whole brain lysate by iTRAQ. Our measurements of α4 and β2 nAChR subunit peptides across the six genotypes using iTRAQ are consistent with published studies on the effect of subunit null-mutation on mature β2* nAChR subtype expression. Importantly, our measures indicate that in the absence of a partner subunit, individual nAChR subunit monomers contributing to heteromeric α4β2* nAChRs are not apparent, and that multi-subunit complexes are required to prevent rapid degradation of free subunits.

nAChR peptides have been recognized previously by mAbs in knockout mouse tissue [30]. The genomic DNA encoding the majority of the extracellular domain of the β2 nAChR subunit (recognized by mAb295) is not removed by exon deletion,

through which the α4 and β2 nAChR subunit knockout mice were generated [4,25], so identification of low levels of α4 and β2 nAChR subunit peptides in their respective KO mice is not surprising. It is also possible that some of the peptides recovered in the α4 and β2 KO samples are incorrectly identified as a result of chimeric spectra in MS/MS that do not actually represent nAChR subunit peptides; however, chimeric spectra generally result in uncertainty of protein identification, rather than positive identification of peptides that are not actually present in the sample [32].

It is possible that truncated nAChR subunit peptides in KO tissue cannot form binding sites but retain some features of nascent nAChR assembly intermediates, since measurable [³H]-epibatidine binding sites decreased in gene-dose-dependent fashion following nAChR subunit deletion, while the amount of total eluted protein following mAb295 affinity purification did not change. In addition, when comparing functions of proteins identified in the dataset adjusted for improper cellular compartment to those in the dataset adjusted for correlation with β2 nAChR subunit expression, proteins serving chaperone isomerase, and ER-Golgi transport functions are lost. Therefore, proteins captured from detergent extracts of KO brain homogenates that do not follow the regression trend likely represent proteins that are associated with incomplete/immature β2* nAChRs, while the more strongly and significantly correlated proteins potentially interact with mature receptors. Proteins negatively correlated with nAChR subunit levels may be involved in degradation and/or compartmentalization of non-functional nAChR proteins, or

Table 3 Proteins with their abundances significantly positively correlated with that of β2 nAChR subunit across genotypes

Correlation coefficient	N	F score	P value	Protein	UniProtKB accession No.	Cellular compartment	Previously identified?	Molecular function
0.748	12	20.268	0	Glial fibrillary acidic protein	P03995	Cytoplasm	No	Protein binding, structural molecule
0.858	18	44.542	0	nAChR subunit α4	O70174	Cell junction	No	Neuro-transmitter receptor
1	18	–	0	nAChR subunit β2	Q9ERK7	Cell junction	No	Neuro-transmitter receptor
0.652	18	11.844	0.003	Neurofilament light poly peptide	P08551	Growth cone	No	Protein binding, structural molecule
0.645	18	11.404	0.004	Actin-related protein 3	Q99JY9	Cytoplasm	No	Nucleotide binding, protein binding
0.637	18	10.904	0.004	Calcium/calmodulin-dependent protein kinase type II subunit α	P11798	Cytoplasm	No	Transferase, nucleotide binding, protein binding
0.917	18	21.235	0.01	Calcium/calmodulin-dependent protein kinase type II subunit γ	Q923T9	Sarcoplasmic reticulum membrane	No	Transferase, nucleotide binding, protein binding
0.57	18	7.681	0.014	F-actin-capping protein subunit α2	P47754	Cytoplasm	No	Protein binding
0.562	18	7.386	0.015	Thyroid hormone receptor- associated protein 3	Q569Z6	Nucleus	No	Nucleotide binding, protein binding
0.665	12	7.933	0.018	Transcriptional activator protein Pur-α	P42669	Nucleus	No	Nucleic acid binding, translation regulator, protein binding
0.539	18	6.563	0.021	Ectonucleotide pyrophosphatase/phosphodiesterase family member 6	Q8BGN3	Cell membrane	No	Catalytic activity, hydrolase activity
0.519	18	5.884	0.027	Spectrin β chain, brain 1	Q62261	Cytoplasm	No	Protein binding, lipid binding, structural molecule activity
0.856	6	11.009	0.029	Ras-related protein Rap-1A	P62835	Cell membrane	No	Hydrolase activity, protein binding, nucleotide binding
0.512	18	5.695	0.03	Myosin-10	Q61879	Cytoplasm	No	Protein binding, nucleotide binding, hydrolase
0.506	18	5.496	0.032	Myelin proteolipid protein	P60202	Cell membrane	No	Structural molecular, protein binding
0.502	18	5.378	0.034	Spectrin α chain, brain	P16546	Cytoplasm	Yes	Hydrolase, protein binding, nucleotide binding
0.493	18	5.149	0.037	Tubulin β-3 chain	Q9ERD7	Cytoplasm	No	Hydrolase, nucleotide binding, structural molecular, protein binding, peptide
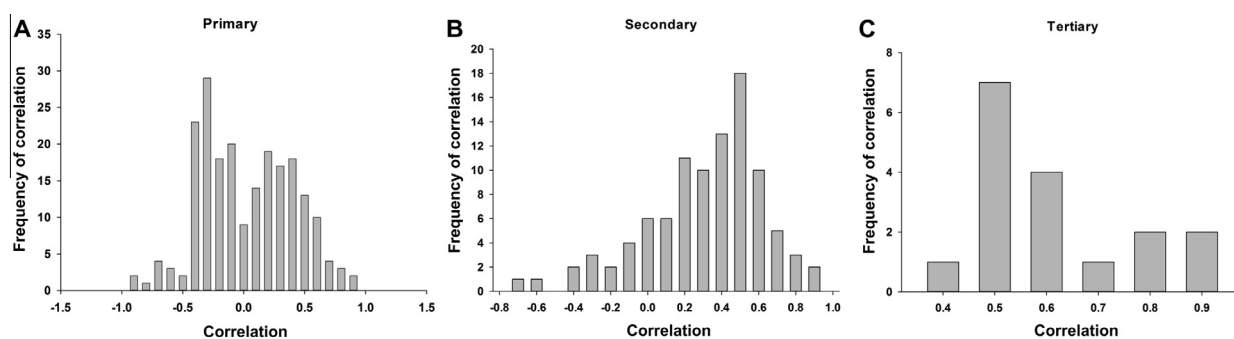
Figure 3 Frequency distribution of correlations for proteins associated with β2 subunit

Frequency distribution of calculated correlations between relative abundances of putative interacting proteins and β2 nAChR log$_2$MRIPA was shown. **A.** The primary dataset (no protein exclusion) is bimodal, indicating the presence of a substantial number of proteins identified with no significant correlation or a negative correlation. **B.** The major (negative correlation) mode is lost when identified proteins in cellular compartments that do not normally contain nAChRs are removed (secondary dataset), resulting in a skewed distribution. **C.** The tertiary dataset (significantly correlated proteins) is also predictably skewed, indicating that the edited dataset favors proteins that are enriched for the β2 nAChR subunit.

may bind to mAb295 and accumulate in the absence of bound nAChRs.

The use of iTRAQ coupled with α4 and β2 nAChR subunit transgenic mouse tissue provides a significant technical advance over previous proteomic methods used to identify specific nAChR-interacting proteins. Separating samples with difference in gel electrophoresis (DIGE) and eliminating bands/spots that appear in the KO control condition prior to LC–MS/MS pose the risk of missing significantly-associated proteins that are expressed in low abundance and may co-migrate with non-specifically captured proteins [33]. Mulitplexing with iTRAQ and identifying as many proteins as possible in the post-IP eluent reduce the risk of missing proteins of interest due to preprocessing steps like DIGE, but increase the risk of identifying proteins that are not necessarily associated with assembled α4β2* nAChRs. Combining SILAC with siRNA-mediated knockdown reduces identification of false interacting proteins, which is not suited to tissue samples and is limited to a direct comparison of two samples [22]. To address this issue, we took advantage of quantitation using iTRAQ to generate linear regression of the apparent abundance of each identified protein together with that of the β2 nAChR subunit across the six genotypes examined in each sample set, allowing us to identify a continuum of protein associations, ranging from highly positive to highly negative correlations.

Previously suggested nAChR-interacting proteins were lost from the dataset as our analysis became more stringent. Eight (out of 17 in total) of α4β2 nAChR-interacting proteins identified by MALDI–ToF-ToF [20] are retained when identified proteins are restricted by cellular compartments, and 1 (out of 17) is identified when only proteins whose expression were significantly correlated with β2 nAChR subunit expression levels were considered, suggesting that these previous analyses may have suffered from missed identification and potentially false positive interactions. The current method, in contrast to MALDI–ToF-ToF [20], identified a significant correlation between the relative abundance of α4 nAChR subunit and the abundance of its primary partner β2 ($r = 0.858$). It is important to note that proteins listed in a recent comprehensive review (2011) [34] include those whose interactions are inferred from modulatory interactions (as with protein kinases and

phosphatases which are known to phosphorylate or dephosphorylate the nAChRs). Such interactions are transient and may be cell-type specific. Therefore, future studies using enriched samples from a particular brain region and/or neuronal phenotype will be required to validate such associations.

Interpretation of interacting proteins that are not likely to interact in functionally relevant ways with target proteins is a caveat in current proteomic methods. This highlights the need to curate results of these analyses carefully and is part of the tradeoff for enhanced discovery and unbiased identification of novel interacting proteins. Examining the relative subcellular distribution of identified proteins in each of the lists generated by increasingly stringent criteria provided some interesting insights. Culling proteins by cellular compartment resulted in a dataset of 91 identified proteins in which 68% were cytoplasmic. Some Golgi/ER membrane resident proteins were also identified, indicating that the list of 91 interacting proteins likely includes proteins that interact with β2* nAChRs during assembly or maturation. The relative subcellular distribution of nAChRs in neurons *in vivo* is unknown, but cell surface expression of α4β2* nAChRs varies both by brain region and model organism [35,36]. The list of 17 proteins whose expression is correlated significantly with that of β2 nAChR subunit eliminates the Golgi/ER resident proteins, suggesting that this group represents proteins that largely interact with mature nAChRs present in the plasma membrane. Interactions with other plasma-membrane resident proteins are likely disrupted following solubilization. This is reflected in the list of 91 interacting proteins, where the majority (65%) are cytoplasmic proteins, indicating that in the mature state, the large cytoplasmic loop of each subunit that resides between transmembrane domains 3 and 4 represents the primary site for intracellular protein–protein interactions.

Establishing molecular function classifications with PANTHER pathway analysis [29] reveals that the primary interactions of mature β2* nAChRs occur with structural proteins that are part of, and regulate the growth and assembly of, the cytoskeleton. These data are consistent with studies showing that β2* nAChRs are involved in production and maintenance of dendritic spines during development [37]. Of particular interest are the cytoskeletal proteins that appear to

play functional roles in the growth and reorganization of synaptic processes, such as actin-related protein 3 (Arp3) and F-actin capping protein subunit α2. Arp3 contributes directly to axon branching [38] and is implicated in strain differences in hippocampal information processing [39]. Activity-dependent accumulation of F-actin capping proteins occurs in dendritic spines [40], supporting the idea that β2* nAChRs play a role in dynamic neuronal cytoarchitecture remodeling and providing a potential molecular mechanism for future evaluation.

Two isoforms of calcium/calmodulin-dependent protein kinase II (CaMKII), α and γ, were identified in the current experiment. CamKII is involved in nAChR recycling [41] and α-kinase-anchoring protein (αKAP, a CaMKII anchoring protein) inhibits proteasomal degradation of muscle-type nAChRs [42]. CaMKII is also a critical mediator of long-term potentiation (LTP) (see [43] for review), a molecular mechanism underlying memory storage. CaMKIIα is specifically associated with the postsynaptic density in excitatory neurons (see [44] for review) and previous studies have demonstrated that acute nicotine exposure in mice activates CaMKII in the spinal cord and brain, which requires activation of β2* nAChRs [45,46]. In addition, β2* nAChR-mediated activation of CaMKII is an essential component of the antinociceptive effects of nicotine [47] and affective signs of nicotine withdrawal [48]. Chronic nicotine exposure results in an increase in CaMKIIα expression and function in nucleus accumbens of mice and this effect is attenuated following administration of a β2 nAChR selective antagonist [49]. Nicotine also influences several aspects of hippocampal-dependent learning [50]. Identification here of a direct association between α4β2* nAChRs and CaMKIIα provides rationale for future studies of its role in hippocampal plasticity.

It should be noted that glial fibrillary acidic protein (GFAP) is one of the most highly correlated proteins identified in the curated list of proteins. Homomeric α7 nAChRs have been reported to be expressed on astrocytes [51]. However evidence of α4β2 nAChR expression on non-neuronal CNS cells is lacking. Identification of GFAP in this study may imply that α4β2* nAChRs could participate in neuron–glia interactions.

In conclusion, we have identified a novel set of nAChR-interacting proteins that are consistent with known nAChR-mediated functions, as well as previously identified interactors such as spectrin-α, validating our methodology. In addition to these biological findings, development of the iTRAQ technique in combination with evaluation in knockout mouse lines will be important for identifying protein–protein interaction without prior knowledge of the complex and for identifying interactions that cannot be detected using traditional protein identification techniques. Identification of an nAChR-associated proteome also provides a set of novel targets for drug discovery of therapeutics for smoking cessation and psychiatric or neurological disorders associated with nicotinic dysfunction. Ultimately, generation of small molecules that are capable of disrupting or facilitating interactions between nAChRs and specific associated proteins holds the promise of providing more targeted therapies with higher selectivity for particular nAChR-mediated behavioral functions and fewer side effects.

Materials and methods

Chemicals

Unless stated otherwise, all reagents were obtained from Sigma Aldrich (St. Louis, MO). [³H]-epibatidine (62.2 Ci/mmol) was purchased from PerkinElmer, Sheldon, CT. iTRAQ reagents were obtained from AB Sciex (Framingham, MA).

Animals

Homozygous wild type (WT), heterozygous (HET) and homozygous (KO) mice lacking either α4 or β2 nAChR subunit were used in the study. β2 nAChR subunit [4] and α4 nAChR subunit [25] knockout (KO) mice were backcrossed at least 30 generations to a C57 BL/6 background. Mice were bred at the University of Colorado, Boulder, housed in groups of no more than 5 individuals per cage, maintained on a 12:12 h light:dark cycle and given *ad libitum* access to food and water. All protocols involving animals were approved by the Institutional Animal Care and Use Committee (IACUC) of Yale University and the University of Colorado and conformed to the standards for animal care and use set by the National Institutes of Health.

Preparation of brain tissue extracts for immunoprecipitation

Animals were sacrificed by cervical dislocation and brains were rapidly placed on an ice-cold surface. After rinsed in chilled phosphate buffer solution (PBS, pH 7.4; containing 136.9 mM NaCl, 2.68 mM KCl, 10.14 mM Na_2HPO_4 and 1.76 mM KH_2PO_4) to carefully wash off any debris, brains were then snap frozen by immersion in −35 °C isopentane and kept frozen at −80 °C until use. On the day of tissue preparation, brains were thawed on a chilled surface and cerebellum was removed and discarded. The resulting tissue (whole forebrain) was homogenized by hand with 37 strokes in a glass tissue grinder in 10 volumes of extraction buffer (EB) (0.6% Triton X-100, 121.9 mM NaCl, 2.68 mM KCl, 10.14 mM Na_2HPO_4, 1.76 mM KH_2PO_4, 5 mM EDTA, 5 mM EGTA, 5 mM NaF, 0.1 mM Na_3VO_4, 1.0 mM PMSF and 10 μg/ml each of aprotonin, prepstatin A and leupeptin; pH 7.4). The resulting homogenate was incubated at 23 °C with gentle rotation for 30 min to facilitate protein solubilization, then subjected to centrifugation for 20 min at 5000 *g*, 4 °C. The resulting supernatant was used for all subsequent experiments.

[³H]-Epibatidine binding from mouse brain extracts

Measurement of the amount of high-affinity nAChRs in brain extracts was performed essentially as described previously [52], except that 1 nM [³H]-epibatidine was used as the radioligand instead of 200 pM [¹²⁵I]-epibatidine. [³H]-epibatidine labeled nAChRs were captured by filtration through a Packard Filtermate 196 Cell Harvester (Meriden, CT) onto Pall type A/D filters pre-soaked in 0.5% polyethylinimine. After washing three times with ice-cold wash buffer (140 mM NaCl, 1.5 mM KCl, 2.0 mM $CaCl_2$, 1.0 mM $MgSO_4$·7H2O, 25 mM HEPES, pH 7.5), radioactivity on individual filters was measured by liquid

scintillation counting on a Beckmann LS6000LL (Indianapolis, IN) at 55% efficiency.

Immunoprecipitation

mAb295 has been previously characterized as an antibody specific to $\beta2^*$ nAChRs [1]. A solid phase mAb295 immunopurification matrix was prepared using M270 Dynabeads (Invitrogen) according to the manufacturer's instructions and stored in PBS containing 0.5% Triton X-100 and 0.02% NaN_3 at 4 °C until use. On the day of IP, bead suspensions were aliquoted, separated on a magnetic stand, and rinsed once with PBS prior to the addition of brain supernatant. IP took place overnight at 4 °C with gentle rotation. Following IP, beads were separated with a magnetic stand and the supernatant was aspirated and discarded. Beads were then rinsed twice with PBS containing 0.01% Tween-20, then again in PBS only. Proteins were eluted from rinsed beads with 500 µl elution buffer (0.5 M NH_4OH and 0.5 mM EDTA) by incubation at 23 °C for 20 min with gentle rotation. Elution was repeated one more time. The resulting eluate was then combined and lyophilized in a Speedvac DNA120 overnight. The lyophilized proteins were used for subsequent proteomic analysis.

iTRAQ labeling and protein identification by LC–MS/MS

All samples were prepared for iTRAQ analysis using a $CHCl_3/$MeOH precipitation after diluting each to 100 µl with water. 400 µl of MeOH was then added and vortexed extensively prior to the addition of 100 µl $CHCl_3$. An additional 300 µl of water was added prior to vortexing and centrifuging at 14,000g for 1 min. The top aqueous layer was removed and discarded and an additional 400 µl MeOH was added. After a 2 min centrifugation at 14,000 g, the MeOH was removed without disturbing the pellet. The pellet was dried in a Speedvac and dissolved in 50 µl of 0.5 M tetraethylammonium bicarbonate (TEAB) with 0.2% SDS. Table S3 lists the amount of each sample used per sample set for labeling which was determined based on a nanodrop measurement at A_{280}versus a buffer blank. Disulfide reduction was performed by incubating with 5 mM tris(2-carboxyethyl)phosphine (TCEP) at 60 °C for 1 h. Alkylation was then performed by incubating with 20 mM methylmethanethiolsulfonate (MMTS) at room temperature for 10 min. Samples were digested using a 1:10 weight/weight ratio protein/trypsin and incubating at 37 °C for 16 h. Each dried iTRAQ label was dissolved in 50 µl of 100% isopropanol. Reporter ion tags and sample identifications are listed in Table S3. After vortexing, each reconstituted iTRAQ reagent was transferred to the appropriate vial and incubated at room temperature for 2 h. At this point, the tagged sample digests were mixed together in each indicated set. 100 µg of sample mixture was then passed over a cation exchange cartridge (AB Sciex) to remove unreacted reagent. The sample was diluted with 2 mL of 10 mM KH_2PO_4/25% acetonitrile (ACN) (pH 3.0) prior to passing over the cation exchange cartridge (conditioned with 10 mM KH_2PO_4/ 25% ACN, pH 3.0). The cartridge was then washed with 1 mL of the same buffer prior to eluting the peptides with 500 µl 10 mM KH_2PO_4, 25% ACN, 350 mM KCl (pH 3.0). The samples were dried, dissolved in 20 µl 70% formic acid (FA) and

diluted with 300 µl 0.1% trifluoroacetic acid (TFA), prior to desalting using a Macrospin C18 (The Nest Group, # SMM SS18V). The bound peptides were eluted with 360 µl of 80% ACN containing 0.1% TFA and the elution was repeated by washing with an additional 180 µl of same solution. Samples were dried in a Speedvac and dissolved in 3 µl FA mixed with 8 µl 0.1% TFA.

Mass spectrometric analysis was performed on an AB Sciex TripleTOF 5600 which is equipped with a Waters nanoAcquity UPLC system, and uses a Waters Symmetry C18 180 µm × 20 mm trap column and a 1.7 µm, 75 µm × 150 mm nanoAcquity UPLC column (45 °C) for peptide separation with the following multiplexed groups: *Set 1 with 6 plex* containing α4WT1, α4HET1, α4KO1, β2WT1, β2HET1 and β2KO1; *Set 2 with 6 plex* containing α4WT2, α4HET2, α4KO2, β2WT2, β2HET2 and β2KO2, and *Set 3 with 6 plex* containing α4WT3, α4HET3, α4KO3, β2WT3, β2HET3 and β2KO3.

Trapping was done at 15 µl/min, 99% Buffer A (99.9% water and 0.1% FA) for 1 min. Peptide separation was performed at 500 nl/min with Buffer A and Buffer B (99.925% and 0.075% FA). The gradient was 99% A at initial conditions with a linear gradient to 35% B at 160 min, and 95% B at 160.3 min. Protein identification and iTRAQ quantitation was performed using AB SCIEX ProteinPilot ver 4.2, which employs a Paragon algorithm with hybrid sequence tag and feature probability database searches [53]. Hence, specific details such as mass tolerances, specific modifications, *etc.* are not used. All iTRAQ results were uploaded into the Yale protein expression database (YPED; http://yped.med.yale.edu/repository/) [54].

Data analysis

Ligand binding and immunoprecipitation

Ligand binding results were transformed from counts per minute (CPM) to fmol of bound ligand for all quantitations. To determine the maximally effective ratio of mAb bead volume for quantitative immunoprecipitation, the average depletion of nicotinic binding sites relative to the input was calculated using a 3-component hyperbolic equation $y = y_0 + a(x)/[b + (x)]$, where "y" is bound ligand captured with residual binding "y_0", maximal depletion "a" at ½ maximal [bead] "b" and [mAb] "x". Curve fits were performed with the above-mentioned equation in SigmaPlot 2001. Statistical significance of the influence of genotype and/or antibody capture efficiency was determined by Student's *t*-test or a one-way ANOVA (when comparing two or more groups, respectively) conducted with SPSS19 with a confidence interval set at 95%.

iTRAQ data analysis

For relative quantitation of proteins identified by LC–MS/MS, the quantified proteins should have a confidence interval for positive identification greater than 95% with at least two unique peptides contributing to the identification. The reporter ion peak areas for each peptide measured were averaged for each protein identified in every group to provide an MRIPA. A control mean for every identified protein was generated by averaging the MRIPA for the two nAChR wild type control animals (α4WT and β2WT). All samples within a set were divided by these control means in order to calculate the ratios of

MRIPA in relative to an averaged control set. The ratio of each identified protein to the level of nAChR proteins was then $\log_2$ transformed and used to measure the relative quantitative expression. Except where indicated, $\log_2$MRIPA was used in all statistical analyses of iTRAQ data within this study. For regression analysis across biological replicates, $\log_2$MRIPA of each protein was correlated with that of the β2 nAChR subunit. Regression and correlation analysis was conducted using SPSS 19 with a confidence interval set at 95%. The frequency distribution of identified proteins was interrogated using the Shapiro–Wilk test of normality with a confidence interval set at 95%.

Authors' contributions

McClure-Begley TD: experiment inception and design, principal author, sample preparation and pharmacological quantitation, and data analysis; Stone KL: preparation of samples for LC–MS/MS, data acquisition and manuscript review; Marks MJ and Grady SR: experiment design, animal production, tissue collection and manuscript review; Colangelo CM: LC–MS/MS data preparation, data analysis and manuscript review; Lindstrom JM: antibody production, experiment design and manuscript review; Picciotto MR: experiment inception and design and manuscript review. All authors read and approved the final manuscript.

Competing interests

Authors declare no competing interests.

Acknowledgements

Supplementary material

Supplementary data associated with this article can be found, in the online version, at http://dx.doi.org/10.1016/j.gpb.2013.05.005.

References

[1] Whiting PJ, Lindstrom JM. Characterization of bovine and human neuronal nicotinic acetylcholine receptors using monoclonal antibodies. J Neurosci 1988;8:3395–404.

[2] Zoli M, Léna C, Picciotto MR, Changeux JP. Identification of four classes of brain nicotinic receptors using beta2 mutant mice. J Neurosci 1998;18:4461–72.

[3] Gotti C, Moretti M, Meinerz NM, Clementi F, Gaimarri A, Collins AC, et al. Partial deletion of the nicotinic cholinergic receptor alpha 4 or beta 2 subunit genes changes the acetylcholine sensitivity of receptor-mediated ^{86}Rb$^+$ efflux in cortex and thalamus and alters relative expression of alpha 4 and beta 2 subunits. Mol Pharmacol 2008;73:1796–807.

[4] Picciotto MR, Zoli M, Léna C, Bessis A, Lallemand Y, Le Novère N, et al. Abnormal avoidance learning in mice lacking functional high-affinity nicotine receptor in the brain. Nature 1995;374:65–7.

[5] Millar NS, Gotti C. Diversity of vertebrate nicotinic acetylcholine receptors. Neuropharmacology 2009;56:237–46.

[6] Cahill K, Stead LF, Lancaster T. Nicotine receptor partial agonists for smoking cessation. Cochrane Database Syst Rev 2012;4:CD006103.

[7] Ago Y, Koda K, Takuma K, Matsuda T. Pharmacological aspects of the acetylcholinesterase inhibitor galantamine. J Pharmacol Sci 2011;116:6–17.

[8] Quik M, Wonnacott S. α6β2* and α4β2* nicotinic acetylcholine receptors as drug targets for Parkinson's disease. Pharmacol Rev 2011;63:938–66.

[9] Mineur YS, Picciotto MR. Nicotine receptors and depression: revisiting and revising the cholinergic hypothesis of depression. Trends Pharmacol Sci 2010;31:580–6.

[10] Bacher I, Rabin R, Woznica A, Sacco KA, George TP. Nicotinic receptor mechanisms in neuropsychiatric disorders: therapeutic implications. Primary Psychiatry 2010;17:35–41.

[11] Bermudez I, Moroni M. Phosphorylation and function of alpha4beta2 receptor. J Mol Neurosci 2006;30:97–8.

[12] Exley R, Moroni M, Sasdelli F, Houlihan LM, Lukas RJ, Sher E, et al. Chaperone protein 14-3-3 and protein kinase A increase the relative abundance of low agonist sensitivity human alpha 4 beta 2 nicotinic acetylcholine receptors in Xenopus oocytes. J Neurochem 2006;98:876–85.

[13] Zhao CJ, Noack C, Brackmann M, Gloveli T, Maelicke A, Heinemann U, et al. Neuronal Ca^{2+} sensor VILIP-1 leads to the upregulation of functional alpha4beta2 nicotinic acetylcholine receptors in hippocampal neurons. Mol Cell Neurosci 2009;40:280–92.

[14] Pollock VV, Pastoor T, Katnik C, Cuevas J, Wecker L. Cyclic AMP-dependent protein kinase A and protein kinase C phosphorylate alpha4beta2 nicotinic receptor subunits at distinct stages of receptor formation and maturation. Neuroscience 2009;158:1311–25.

[15] Eilers H, Schaeffer E, Bickler PE, Forsayeth JR. Functional deactivation of the major neuronal nicotinic receptor caused by nicotine and a protein kinase C-dependent mechanism. Mol Pharmacol 1997;52:1105–12.

[16] Fenster CP, Beckman ML, Parker JC, Sheffield EB, Whitworth TL, Quick MW, et al. Regulation of alpha4beta2 nicotinic receptor desensitization by calcium and protein kinase C. Mol Pharmacol 1999;55:432–43.

[17] Marszalec W, Yeh JZ, Narahashi T. Desensitization of nicotine acetylcholine receptors: modulation by kinase activation and phosphatase inhibition. Eur J Pharmacol 2005;514:83–90.

[18] Tannu NS, Hemby SE. Methods for proteomics in neuroscience. Prog Brain Res 2006;158:41–82.

[19] Williams K, Wu T, Colangelo C, Nairn AC. Recent advances in neuroproteomics and potential application to studies of drug addiction. Neuropharmacology 2004;47:148–66.

[20] Kabbani N, Woll MP, Levenson R, Lindstrom JM, Changeux JP. Intracellular complexes of the beta2 subunit of the nicotinic acetylcholine receptor in brain identified by proteomics. Proc Natl Acad Sci U S A 2007;104:20570–5.

[21] Selbach M, Mann M. Protein interaction screening by quantitative immunoprecipitation combined with knockdown (QUICK). Nat Methods 2006;3:981–3.

[22] Mittler G, Butter F, Mann M. A SILAC-based DNA protein interaction screen that identifies candidate binding proteins to functional DNA elements. Genome Res 2009;19:284–93.

[23] Luo R, Colangelo CM, Sessa WC, Zhao H. Bayesian analysis of iTRAQ data with nonrandom missingness: identification of differentially expressed proteins. Stat Biosci 2009;1:228–45.

[24] Hill EG, Schwacke JH, Comte-Walters S, Slate EH, Oberg AL, Eckel-Passow JE, et al. A statistical model for iTRAQ data analysis. J Proteome Res 2008;7:3091–101.

[25] Ross SA, Wong JY, Clifford JJ, Kinsella A, Massalas JS, Horne MK, et al. Phenotypic characterization of an alpha 4 neuronal nicotinic acetylcholine receptor subunit knock-out mouse. J Neurosci 2000;20:6431–41.

[26] Whiteaker P, Cooper JF, Salminen O, Marks MJ, McClure-Begley TD, Brown RW, et al. Immunolabeling demonstrates the interdependence of mouse brain alpha4 and beta2 nicotinic acetylcholine receptor subunit expression. J Comp Neurol 2006;499:1016–38.

[27] Consortium UniProt. Reorganizing the protein space at the Universal Protein Resource (UniProt). Nucleic Acids Res 2012;40:D71–5.

[28] Johnson EM, Kinoshita Y, Weinreb DB, Wortman MJ, Simon R, Khalili K, et al. Role of Pur alpha in targeting mRNA to sites of translation in hippocampal neuronal dendrites. J Neurosci Res 2006;83:929–43.

[29] Thomas PD, Kejariwal A, Campbell MJ, Mi H, Diemer K, Guo N, et al. PANTHER: a browsable database of gene products organized by biological function, using curated protein family and subfamily classification. Nucleic Acids Res 2003;31:334–41.

[30] Jones IW, Wonnacott S. Why doesn't nicotinic ACh receptor immunoreactivity knock out? Trends Neurosci 2005;28:343–5.

[31] Gotti C, Clementi F, Fornari A, Gaimarri A, Guiducci S, Manfredi I, et al. Structural and functional diversity of native brain neuronal nicotinic receptors. Biochem Pharmacol 2009;78:703–11.

[32] Houel S, Abernathy R, Renganathan K, Meyer-Arendt K, Ahn NG, Old WM. Quantifying the impact of chimera MS/MS spectra on peptide identification in large scale proteomics studies. J Proteome Res 2010;6:4152–60.

[33] Wu WW, Wang G, Baek SJ, Shen RF. Comparative study of three proteomic quantitative methods, DIGE, cICAT, and iTRAQ, using 2D gel- or LC–MALDI TOF/TOF. J Proteome Res 2006;5:651–8.

[34] Jones AK, Buckingham SD, Sattelle DB. Proteins interacting with nicotinic acetylcholine receptors: expanding functional and therapeutic horizons. Trends Pharmacol Sci 2010;31:455–62.

[35] Hill Jr JA, Zoli M, Bourgeois JP, Changeux JP. Immunocytochemical localization of a neuronal nicotinic receptor: the beta 2-subunit. J Neurosci 1993;13:1551–68.

[36] Zambrano CA, Salamander RM, Collins AC, Grady SR, Marks MJ. Regulation of the distribution and function of [(125)I] epibatidine binding sites by chronic nicotine in mouse embryonic neuronal cultures. J Pharmacol Exp Ther 2012;342:245–54.

[37] Lozada AF, Wang X, Gounko NV, Massey KA, Duan J, Liu Z, et al. Induction of dendritic spines by β2-containing nicotinic receptors. J Neurosci 2012;32:8391–400.

[38] Spillane M, Ketschek A, Jones SL, Korobova F, Marsick B, Lanier L, et al. The actin nucleating Arp2/3 complex contributes to the formation of axonal filopodia and branches through the regulation of actin patch precursors to filopodia. Dev Neurobiol 2011;71:747–58.

[39] Pollak DD, John J, Scharl T, Leisch F, Schneider A, Hoeger H, et al. Strain-dependent regulation of neurotransmission and actin-remodelling proteins in the mouse hippocampus. Genes Brain Behav 2006;5:200–4.

[40] Kitanishi T, Sakai J, Kojima S, Saitoh Y, Inokuchi K, Fukaya M, et al. Activity-dependent localization in spines of the F-actin capping protein CapZ screened in a rat model of dementia. Genes Cells 2010;15:737–47.

[41] Martinez-Pena y Valenzuela I, Mouslim C, Akaaboune M. Calcium/calmodulin kinase II-dependent AChR cycling at the mammalian neuromuscular junction in vivo. J Neurosci 2010;30:12455–65.

[42] Mouslim C, Aittaleb M, Hume RI, Akaaboune M. A role for the CaM kinase II related anchoring protein (αkap) in maintaining the stability of nicotinic acetylcholine receptors. J Neurosci 2012;32:5177–85.

[43] Lisman J, Yasuda R, Raghavachari S. Mechanisms of CaMKII action in long-term potentiation. Nat Rev Neurosci 2012;13:169–82.

[44] Liu XB, Murray KD. Neuronal excitability and calcium/calmodulin-dependent protein kinase type II: location, location, location. Epilepsia 2012;53:45–52.

[45] Damaj MI. Nicotinic regulation of calcium/calmodulin-dependent protein kinase II activation in the spinal cord. J Pharmacol Exp Ther 2007;320:244–9.

[46] Jackson KJ, Walters CL, Damaj MI. Beta 2 subunit-containing nicotinic receptors mediate acute nicotine-induced activation of calcium/calmodulin-dependent protein kinase II-dependent pathways in vivo. J Pharmacol Exp Ther 2009;330:541–9.

[47] Damaj MI. Behavioral modulation of neuronal calcium/calmodulin-dependent protein kinase II activity: differential effects on nicotine-induced spinal and supraspinal antinociception in mice. Biochem Pharmacol 2007;74:1247–52.

[48] Jackson KJ, Damaj MI. L-Type calcium channels and calcium/calmodulin-dependent protein kinase II differentially mediate behaviors associated with nicotine withdrawal in mice. J Pharmacol Exp Ther 2009;330:152–61.

[49] Jackson KJ, Damaj MI. Beta2-containing nicotinic acetylcholine receptors mediate calcium/calmodulin-dependent protein kinase II and synapsis I protein levels in the nucleus accumbens after nicotine withdrawal in mice. Eur J Pharmacol 2013;701:1–6.

[50] Kenney JW, Gould TJ. Modulation of hippocampus-dependent learning and synaptic plasticity by nicotine. Mol Neurobiol 2008;38:101–21.

[51] Teaktong T, Graham AJ, Court JA, Perry RH, Jaros E, Johnson M, et al. Nicotinic acetylcholine receptor immunohistochemistry in Alzheimer's disease and dementia with Lewy bodies: differential neuronal and astroglial pathology. J Neurol Sci 2004;225:39–49.

[52] Marks MJ, McClure-Begley TD, Whiteaker P, Salminen O, Brown RW, Cooper J, et al. Increased nicotinic acetylcholine receptor protein underlies chronic nicotine-induced up-regulation of nicotinic agonist binding sites in mouse brain. J Pharmacol Exp Ther 2011;337:187–200.

[53] Shilov IV, Seymour SL, Patel AA, Loboda A, Tang WH, Keating SP, et al. The Paragon Algorithm, a next generation search engine that uses sequence temperature values and feature probabilities to identify peptides from tandem mass spectra. Mol Cell Proteomics 2007;6:1638–55.

[54] Shifman MA, Li Y, Colangelo CM, Stone KL, Wu TL, Cheung KH, et al. YPED: a web-accessible database system for protein expression analysis. J Proteome Res 2007;6:4019–24.